Inorganic Chemistry

Article

pubs.acs.org/IC

Coordination Polymer Submicrospheres: Fast Microwave Synthesis and Their Conversion under Different Atmospheres

Shengliang Zhong,* Hongyu Jing, Yuan Li, Shungao Yin, Chenghui Zeng, and Lei Wang*

College of Chemistry and Chemical Engineering, Jiangxi Normal University, Nanchang 330022, People's Republic of China

Supporting Information

ABSTRACT: Rare earth (RE) based coordination polymer (CP) submicrospheres have been prepared from pyridine-2,5-dicarboxylic acid and $RE(NO_3)_3$ via a facile microwave heating method in 5 min, with *N*,*N*-dimethylformamide (DMF) as solvent. The submicrospheres have diameters of 100−400 nm. Furthermore, the surface of the microspheres is smooth and the microspheres are solid. Several CP submicrospheres (RE = La, Gd, Y) were selected and calcined under different atmospheres (including air, N_2, and NH_3). After calcination in air at 550 °C for 4 h, rare earth oxide (RE_2O_3) submicrospheres were obtained. On calcination under an N_2 atmosphere, $LaN/La_2O_3/C$ composite spheres were obtained for La-based CPs. For Gd(Y)-based CPs, $Gd_2O_3(Y_2O_3)/C$ composite spheres were obtained. Porous carbon submicrospheres were obtained after the removal of RE_2O_3 and REN from the composite spheres. Interestingly, under an NH_3 atmosphere, $La_2O_2CN_2$ submicrospheres were produced from the La-based CPs. In addition, the Gd-based and Y-based CPs submicrospheres gave $Gd_2O_3/GdN/C$ and Y_2O_3/C submicrospheres, respectively. As examples of their potential applications, their upconversion properties and electrochemical properties of the as-prepared products were investigated. This facile microwave synthesis method may offer an attractive approach for the preparation of other RE-CP micro-/nanostructures, and many interesting materials may be derived.

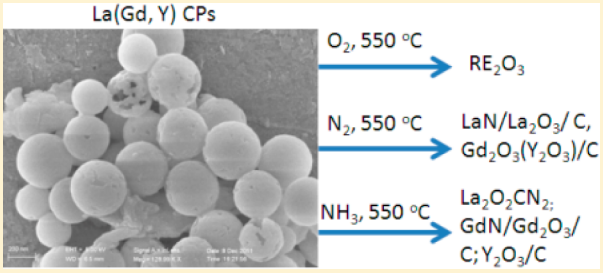

INTRODUCTION

In the past decade, the preparation and application of CPs at the micro-/nanoscale have aroused increasing interest.[1] More and more CPs with various morphologies and structures have been prepared by various methods. For example, CP particles with diameters of a few hundred nanometers were prepared by simple addition of an initiation solvent to a precursor solution of metal ions and metalloligands.[2] Highly monodisperse M^{III}-based soc-MOFs (M = In, Ga) with cubic and truncated cubic morphologies were prepared by a conventional heating method.[3] Ultrathin 2D CP nanosheets were prepared by a microemulsion method.[4] CP hollow spheres with diameters of 260−500 nm have been prepared via a solvothermal method by our group, and the formation mechanism was discussed.[5] As is well known, microwave can be employed to overcome vigorous conditions and long reaction times, because it creates high heating effects in a short time.[6] At the same time, microwave heating may have a beneficial effect on the properties and performance of materials.[7] Microwave heating methods have also found application in the preparation of CP micro-/nanomaterials, and it turned out that these methods could abruptly shorten the preparation time. For instance, three known MOFs, namely IRMOF1, IRMOF2, and IRMOF3, were prepared through a rapid microwave-assisted methodology in 25 s.[8] The morphology design of $Cu_3(btc)_{2n}$ (btc = benzene-1,3,5-tricarboxylate) was realized by microwave irradiation in 60 min. A morphological transition (octahedron−cuboctahedron−cube) was observed.[9] Uniform europium-based infinite CP submicrospheres have been prepared via a facile and fast microwave heating method in 5 min by our group.[10]

Recent work demonstrated that CPs are suitable precursors for the production of nanoscale materials with optimized morphologies and properties. By fine control of the conditions, metals, metal oxides, metal sulfides, and other nanosized materials with different morphologies can be obtained from CP precursors.[11] It turns out that the obtained nanomaterials from nano-CP precursors show better and more useful properties. Among them, CPs have been demonstrated as promising precursors to create functional nanoporous carbons. Several porous carbon materials have been prepared by various methods using coordination polymers as the precursors.[12] For instance, nanoporous carbon prepared by direct carbonization of Al-based porous coordination polymers exhibits superior sensing capabilities toward toxic aromatic substances.[13] Porous carbon with exceptionally high surface area, hydrogen sorption capacity, and excellent electrochemical performance was prepared from highly porous zeolite-type MOF (ZIF-8) and furfuryl alcohol.[14] Thus, far, several MOFs, such as MOF-5, Al-PCP, and ZIF-8, have been demonstrated as promising precursors, yielding highly nanoporous carbons showing excellent properties in gas adsorption, electrochemical capacitance, sensing, and catalysis. Research on the preparation of carbons from CPs has opened up an exciting avenue toward

Received: March 12, 2014
Published: August 1, 2014

   dx.doi.org/10.1021/ic5005769 | *Inorg. Chem.* 2014, 53, 8278−8286

functional carbon-based nanoporous materials. Owing to the unique nature of nanoporous structures, nanoporous carbon is used in many research fields, such as contamination removal, gas storage, supercapacitors, and carriers for drug delivery systems. For example, mesoporous carbon has good electrical properties as an electrode material due to its high specific surface area, plentiful mesoporous structure, and appropriate pore size for rapid mass transfer as well as ion diffusion.[15] The nitrogen-doped porous carbon prepared directly by nitrogen-rich precursors ensures an improved adsorption/absorption for acidic gases such as CO_2.[16] In addition, aligned carbon nanotube and polymer composites are a new class of multifunctional chemical vapor sensors with low power consumption, high sensitivity, good selectivity, and excellent environmental stability, as detailed in a previous report.[17] Because of their excellent properties and broad application, carbon and carbon composites have been intensely investigated. The preparation of carbon-based materials with excellent properties via a facile process has been pursued by many researchers.

Organic ligands in the CPs are abundant in carbon, which is the optimal precursor of carbon composite materials. In addition, the structures and components of the ligands in the CPs are readily tuned. Therefore, CPs is also a good precursor for carbon composite and carbon-related materials. On the basis of the successful preparation by our group of uniform europium-based CP submicrospheres via microwave heating,[10] in this work, other RE-based CP submicrospheres have been prepared by the same method. Subsequently, the as-prepared CP submicrospheres were calcined under atmospheres of air, N_2, and NH_3. A series of carbon and carbon-based materials with interesting structures and compositions were obtained. The as-prepared products were well characterized and analyzed, and their properties were also measured.

EXPERIMENTAL SECTIONS

Preparation. The RE-based CP submicrospheres were prepared by the same method that we reported recently.[10] The detailed process is as follows: 32 mL of a DMF solution containing 0.1 mmol of $RE(NO_3)_3{\cdot}nH_2O$ and 0.3 mmol of pyridine-2,5-dicarboxylic acid was poured into a 100 mL round-bottom flask. The resulting mixture was stirred for 20 min at room temperature and then was heated in a microwave oven for 5 min. The microwave power and frequency were set at 150 W and 2450 MHz. The microwave oven used in our experiments is a modified household microwave oven equipped with a refluxing apparatus. After irradiation, the flask was naturally cooled to room temperature. The precipitates were centrifuged, washed several times with ethanol, and then dried under vacuum at 60 °C overnight. After that, the as-obtained products were thermally treated under different conditions at 550 °C for 4 h.

Characterization. Elemental analysis of C, H, and RE in the solid samples was carried out on a VarioEL instrument (Elementar Analysensysteme GmbH) and an inductive coupled plasma (ICP) atomic emission spectrometer (POEMS, TJA), respectively. X-ray photoelectron spectroscopy (XPS) was performed using a PerkinElmer RBD upgraded PHI-5000C ESCA system with monochromatic Mg Kα excitation, and a charge neutralizer was used to investigate the surface electronic states of the samples. Powder X-ray diffraction (XRD) patterns were obtained with a Rigaku/Max-3A X-ray diffractometer with Cu Kα radiation (λ 1.54178 Å); the operation voltage and current were maintained at 40 kV and 40 mA, respectively. Field emission scanning electron microscopy (FE-SEM) images were obtained with a JEOL JSM-6330F instrument operated at a beam energy of 15.0 kV. Transmission electron microscopy (TEM) images were obtained with a JEOL-2010 TEM instrument at an accelerating voltage of 200 kV. Infrared (IR) spectra were obtained with on a Magna-IR750 FTIR spectrometer as KBr pellets, scanning from 4000 to 400 cm^{-1} at room temperature. Thermogravimetric (TG) analysis was carried out at a constant heating rate of 10 °C min^{-1} from room temperature to 800 °C, using a TA-50 thermal analyzer. Photoluminescence (PL) excitation and emission spectra were measured using a fluorospectrometer (FLUOROLOG-3-TAU). The upconversion emission spectra were measured under 980 nm excitation using a semiconductor laser (power set at 1000 mW) diode in a darkened room. The photoluminescence measurements were measured in the solid state. Before measurement, the samples were prepared by pressing the samples in a stainless sample well.

Electrochemical Measurements. All electrochemical experiments were carried out on a CHI660a electrochemical workstation (Shanghai Chenhua Instruments Co.) at room temperature. The working electrode was prepared by loading a slurry containing 90 wt % of multihole carbon microspheres (about 2 mg), and 10 wt % of poly(vinylidene fluoride) (PVDF) (in *N*-methylpyrrolidone). After the electrode materials were loaded, the working electrode was pressed and dried under vacuum at 80 °C for 12 h. In a three-electrode system, the nickel foam loaded above as the working electrode was investigated with a Pt counter electrode and Ag/AgCl reference electrode in 6 M KOH solution as the electrolyte. CV curves were obtained in the potential range of 0−0.6 V vs Ag/AgCl by varying the scan rate from 5 to 200 mV s^{-1}. Charge/discharge measurements were carried out with a constant current at 0.5−10.0 A g^{-1} with a potential window of 0−0.6 V.

RESULTS AND DISCUSSION

Characterization and Structure of the RE-Based CPs. Figure 1 shows the SEM images of the products prepared after 5 min of microwave heating. It clearly shows that the product is composed of uniform microspheres with diameters ranging from 100 to 400 nm, which is similar to those for the europium-

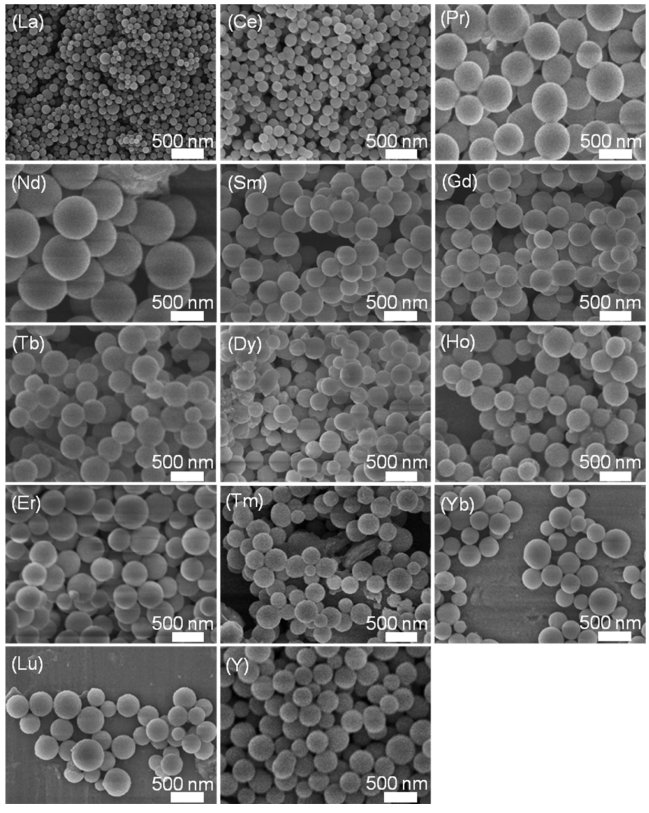

Figure 1. SEM images of RE-CPs obtained after microwave irradiation at 150 W for 5 min.

dx.doi.org/10.1021/ic5005769 | Inorg. Chem. 2014, 53, 8278−8286

based CP submicrospheres reported by us.[10] As is well known, La, Gd, and Y can be denoted as light rare earth, middle rare earth, and heavy rare earth elements, respectively. In this work, the products built from La, Gd, and Y were selected as the representative samples and XRD, IR, TG-DTA, and XPS were used to investigate the composition and structure of the products.

Figure S1 (Supporting Information) shows the representative XRD pattern of the as-prepared La-based, Gd-based, and Y-based products, clearly indicating that they are all amorphous and noncrystalline.[2] The coordination of the carboxylate groups to La^{3+}, Gd^{3+}, and Y^{3+} ions was confirmed by the IR spectra (Figure S2, Supporting Information), as evidenced by a shift in the C═O stretching frequency to 1654 cm^{-1} (La-CPs), 1618 cm^{-1} (Gd-CPs), and 1593 cm^{-1} (Y-CPs) from 1736 cm^{-1} for the uncoordinated building block pyridine-2,5-dicarboxylate.[10] The TG curves taken in air exhibit two main weight losses (Figure S3, Supporting Information). The first weight loss of about 12% before 150 °C corresponds to the loss of water molecules in the product. The second weight loss from 150 to 800 °C is due to the burnout of organic molecules. The survey XPS spectrum reveals that the microspheres are composed of RE, C, N, and O (Figure S4, Supporting Information). From the elemental analysis for La-CPs, Gd-CPs, and Y-CPs, the following data were found: La 29.08%, Gd 32.83%, Y 21.16%; C 27.90%, 23.73%, and 28.68%, respectively; H 2.56%, 2.94%, and 4.90%, respectively; N 4.94%, 4.11%, and 4.67%, respectively. On the basis of the above considerations, the products can be presumed to have the compositions $La_2(C_7H_3NO_4)_3 \cdot nH_2O$, $Gd_2(C_7H_3NO_4)_3 \cdot nH_2O$, and $Y_2(C_7H_3NO_4)_3 \cdot nH_2O$. On the basis of the above analysis, it is safe to draw a conclusion that RE-based CP microspheres have been prepared.

Characterization and Properties of the Product Obtained after Calcination under Different Conditions. *Calcination in the Air.* As discussed before, CPs are suitable precursors for the preparation of nanoamaterials with different compositions by finely controlling the processing conditions. In this work, La-CPs, Gd-CPs, and Y-CPs were selected and calcined under different conditions. Figure 2 is the XRD pattern of the products obtained by calcining the RE-CPs microspheres at 550 °C for 4 h in air. The X-ray diffraction data clearly show that the products are RE_2O_3. All diffraction peaks of the XRD patterns for each sample can be readily indexed as hexagonal La_2O_3 (JCPDS No. 05-0602), cubic Gd_2O_3 (JCPDS No. 43-1014), and cubic Y_2O_3 (JCPDS No. 43-0661), respectively. Figure 3 shows the SEM and TEM images of the rare earth oxide obtained by calcining the RE-CP microspheres at 550 °C for 4 h. It can be seen from Figure 3 that the oxides still maintain spherical structures, indicating that the calcination will not change the morphology of the product. However, their particle size decreased to some extent. Interestingly, by fine observation, the Y_2O_3 spheres are obviously porous.

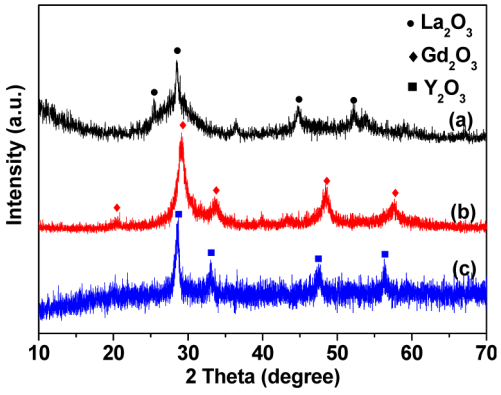

Figure 2. XRD patterns of the products prepared after calcination of the RE-CPs in the air: (a) La-CP; (b) Gd-CP; (c) Y-CP.

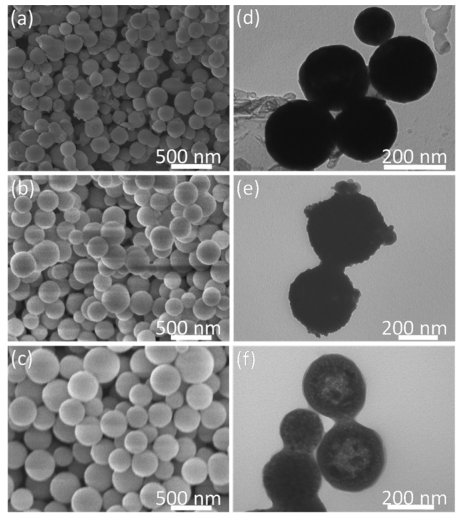

Figure 3. SEM images (a–c) and TEM images (d–f) of the products obtained by calcining the RE-CP microspheres at 550 °C for 4 h: (a, d) La-CP; (b, e) Gd-CP; (c, f) Y-CP.

Calcination under an N_2 Atmosphere. After Calcination under an N_2 Atmosphere. Figure 4 shows the SEM and TEM images of the products after calcination of the RE-CPs under an N_2 atmosphere at 550 °C for 4 h. It clearly demonstrates that the appearance of the products is still spherelike. Elemental analysis results indicate that N (0.87%) and C (6.78%) of the La-CPs are preserved. However, for Gd-based and Y-based CPs, N is 0.14% and 0.23% and C is 4.46% and 5.31%,

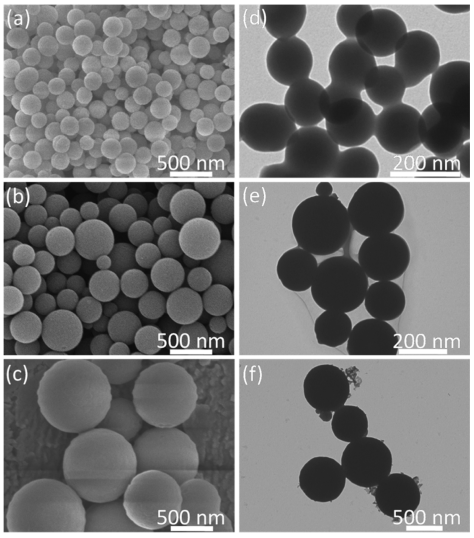

Figure 4. SEM images (a–c) and TEM images (d–f) of the products obtained by calcination of the RE-CP microspheres at 550 °C for 4 h under an N_2 atmosphere: (a, d) La-CP; (b, e) Gd-CP; (c, f) Y-CP.

dx.doi.org/10.1021/ic5005769 | Inorg. Chem. 2014, 53, 8278–8286

respectively. These results suggest that parts of N and C are still in the product after calcination of RE-CPs under an N_2 atmosphere.

XRD results (Figure 5) show that the Gd-CP transforms into Gd_2O_3 (cubic, JCPDS No. 43-1014) after calcination under an

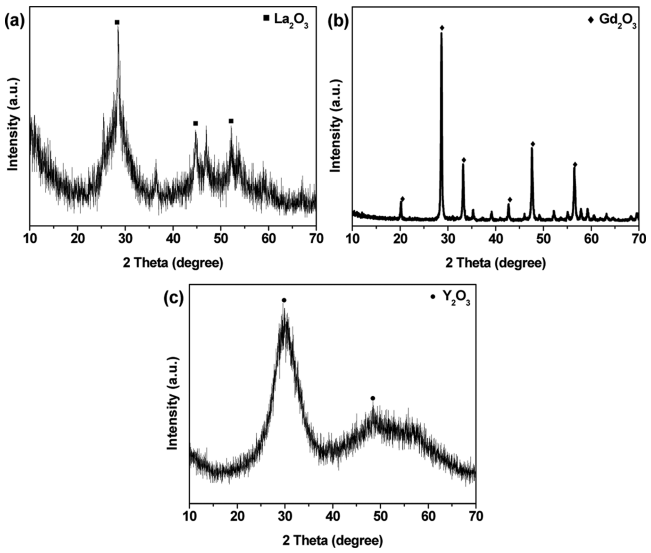

Figure 5. XRD patterns of the products obtained after calcination of the RE-CP microspheres at 550 °C for 4 h under an N_2 atmosphere: (a) La-CP; (b) Gd-CP; (c) Y-CP.

N_2 atmosphere. Furthermore, the peaks are sharp, indicating that the product is quite crystalline. For Y-CP, Y_2O_3 (cubic, JCPDS No. 43-0661) was produced. However, the peaks are broadened to some extent, indicating that the product is not very crystalline. To optimize the calcination protocol, we calcined the Gd-CP at 450, 650, and 750 °C under an N_2 atmosphere for 4 h, respectively. From the XRD patterns (as shown in Figure S5, Supporting Information), the product obtained after calcination at 450 °C is not well crystallized and the product obtained at 650 °C is similar to the product prepared at 550 °C. When the calcination temperature is increased to 750 °C, a mixture of cubic and monoclinic Gd_2O_3 is produced. We can draw the conclusion that the calcination temperature has a great effect on the phase and crystallinitiy of the final product. For La-CP, the major phase is La_2O_3. However, some uncertain impurity peaks are found. As the content of N was high in the product, we think the nitride compound of La may have formed, which will be discussed later.

After Acid Treatment. The La_2O_3 was then etched away from the La sample with 6 mol L^{-1} HNO_3. Figure 6a is the TEM image of the sample treated for 1 day, and Figure 6b is that for 3 days. The morphology of the samples was similar to that of La-CP. However, the products were porous due to the removal of the oxide.

The XRD patterns (Figure 7a) of the products obtained after acid treatment indicated that only amorphous carbon was found after 3 days. In addition, a composite of LaN (cubic, JCPDS No. 15-0892) and amorphous carbon was obtained after treatment for 1 day. LaN has attracted a great deal of research because of its high hardness, brittleness, high melting point, and superconducting transition temperature. This is also interesting from an optical, electronic, magnetic, vibrational, and mechanical properties point of view. We treated the

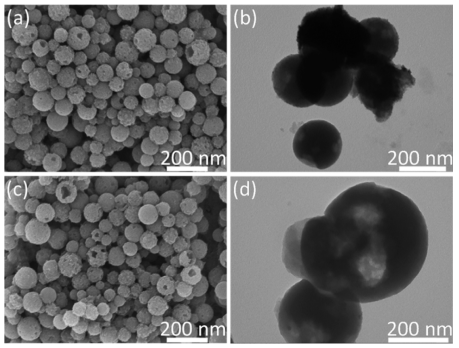

Figure 6. SEM (a, c) and TEM images (b, d) of the products obtained by calcination of La-CP spheres under an N_2 atmosphere after acid treatment: (a, b) samples treated for 1 day; (c, d) samples treated for 3 days.

product with 6 mol L^{-1} NaOH to remove the LaN, and then Nessler's reagent was added to the centrifuged supernatant to test NH_4^+ (Figure 7c). The transparent supernatant generated a tan precipitate immediately, which further proved the existence of LaN. After alkali treatment, the product was a mixture of La_2O_3 and $La(OH)_3$ (Figure 7d).

Raman spectroscopy was used for the characterization of the electronic structure of carbon products, which were treated with acid for 3 days. A change in Raman band intensity and shifts provide information on the nature of C−C bonds and defects. The Raman spectra in Figure 7b show the characteristic D and G bands at 1344 and 1597 cm^{-1} found in the composite. The D band is a common feature for sp^3 defects in carbon, and the G band provides information on in-plane vibrations of sp^2-bonded carbons. The intensity ratio of the D band to the G band usually reflects the order of defects in graphite. The calculated I_D/I_G ratio of the sample was 1.22, and it has been previously reported that an increase in the I_D/I_G ratio during solvothermal processing or chemical reduction is also due to the fragmentation of sp^2 domains in comparison with pure graphite.[18,19] Therefore, the product obtained after calcining La-CPs under N_2 was a mixture of La_2O_3, LaN, and carbon.

Under an NH_3 Atmosphere. After Calcination under NH_3. As is well known, calcining active metal compounds under an NH_3 atmosphere always leads to the formation of nitrides. To the best of our knowledge, calcining MOFs under an NH_3 atmosphere has been rarely studied. In this case, RE-CPs have been calcined under an NH_3 atmosphere at 550 °C for 4 h. Figure 8 gives the SEM and TEM images of the products that were RE-CPs after calcination under an NH_3 atmosphere at 550 °C for 4 h. It can be seen that the appearance of the products was retained. We found that the percentages of N were significantly improved: for La the sample was 11.58% N (0.87% under an N_2 atmosphere), the Gd sample was 2.35% N (0.14% under an N_2 atmosphere), and the Y sample was 0.39% N (0.23% under an N_2 atmosphere). At the same time, the percentage of C was improved as well: for La the sample was 12.86% C (6.78% under an N_2 atmosphere), the Gd sample was 14.00% C (4.46% under an N_2 atmosphere), and the Y sample was 9.92% C (5.31% under an N_2 atmosphere). On the basis of the above analysis, we conjectured that Gd-nitride might form after calcination under the the NH_3 atmosphere. Figure 9 shows the XRD patterns of the products after calcination of La-CP, Gd-CP, and Y-CP under an NH_3 atmosphere. Unexpectedly, $La_2O_2CN_2$ (tetragonal, JCPDS No. 49-1162) was obtained. The synthesis and crystal structure

dx.doi.org/10.1021/ic5005769 | Inorg. Chem. 2014, 53, 8278−8286

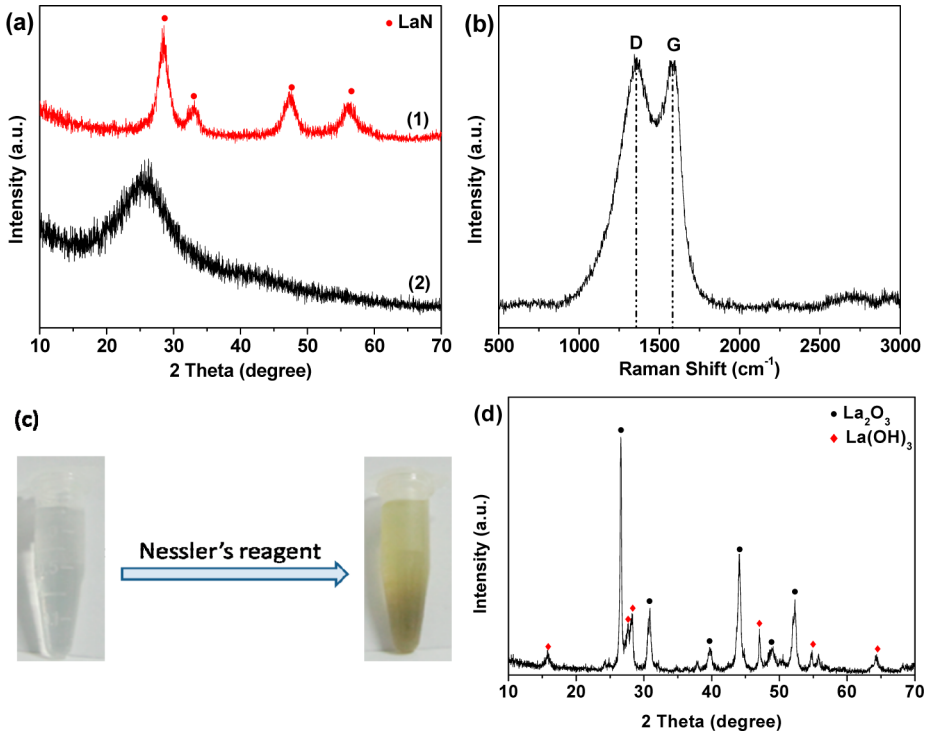

Figure 7. (a) XRD patterns of the product obtained after acid treatment of the sample prepared by calcination of the La-CPs under an N_2 atmosphere: (1) 1 day; (2) 3 days. (b) Raman spectra of the product obtained after acid treatment for 3 days excited with a UV laser at 514 nm. (c) Photographs of the supernatant with alkali treatment before and after addition of Nessler's reagent. (d) XRD pattern of the product obtained after alkali treatment.

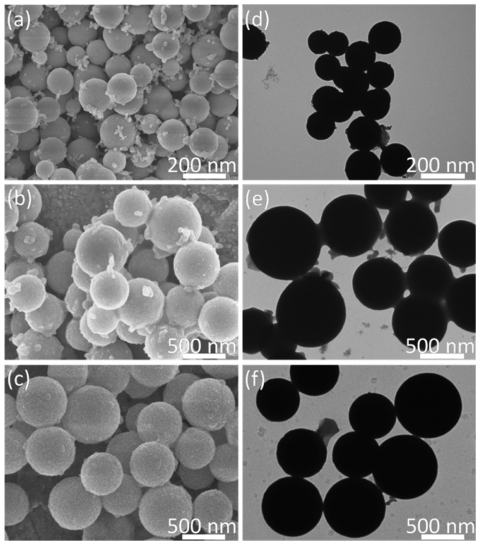

Figure 8. SEM images (a–c) and TEM images (d–f) of the products obtained by calcination of the RE-CP microspheres at 550 °C for 4 h under an NH_3 atmosphere: (a, d) La-CP; (b, e) Gd-CP; (c, f) Y-CP.

refined by the Rietveld method of $La_2O_2CN_2$ have already been reported.[20] Usually, the synthesis required more than 900 °C and 10 h under flowing ammonia. However, $Ln_2O_2CN_2$ exhibits both powerful nitridation and carburization abilities, and several metal nitride and carbide nanoparticles can be easily obtained at temperatures lower than those reported for the conventional methods.[21] In comparison to metal oxides, metal nitride and carbide nanoparticles have superior properties in some respects, such as excellent electronic characteristics, extreme corrosion and wear resistance, and good catalytic properties. According to our experimental results, we found a method that was efficient and had low energy consumption to obtain $Ln_2O_2CN_2$. For Gd-CP and Y-CP, the major phases are Gd_2O_3 and Y_2O_3, respectively. However, some unknown peaks were also found, which will be discussed later.

We treated the Gd sample with 6 mol L^{-1} HNO_3 for 3 days to remove Gd_2O_3. The XRD patterns in Figure 10 showed that the product treated for 1 day was GdN (cubic, JCPDS No. 15-0888) and the product treated for 3 days was carbon, similar to the product obtained after calcining La-CP under an N_2 atmosphere. The results showed that light rare earth elements formed nitrides under an N_2 atmosphere more readily than heavy rare earth elements, and the middle rare earth elements can also form nitrides under an NH_3 atmosphere. However, it is difficult for heavy rare earth elements to form nitrides. We also treated the product of Gd-CP calcination under an NH_3 atmosphere with 6 mol L^{-1} NaOH and Nessler's reagent; the result was consistent with La-CP calcination under an N_2 atmosphere.

The FTIR spectra of the products that were calcined under different atmospheres are given in Figure S6 (Supporting Information). The peak at about 3500 cm^{-1} is attributed to the stretching modes of OH groups associated with the water molecules, and the band at 1500–1600 cm^{-1} belongs to the hydroxyl deformation mode of the water molecules. The strong peaks at 1394, 1384, and 1364 cm^{-1} (Figure S6a) are due to the vibration mode of CO_3^{2-} from CO_2 absorbed on the surface of the materials. The vibration mode of CN in La_2O_3 obtained under an N_2 atmosphere resulted in a peak at 1472 cm^{-1}, but it did not appear in the curves of the Gd and Y samples, testifying that no nitride was formed. The existence of Gd-nitride in the product obtained after calcination under NH_3 can be proved by the band at 1457 cm^{-1} in Figure S6c. There are two

dx.doi.org/10.1021/ic5005769 | Inorg. Chem. 2014, 53, 8278–8286

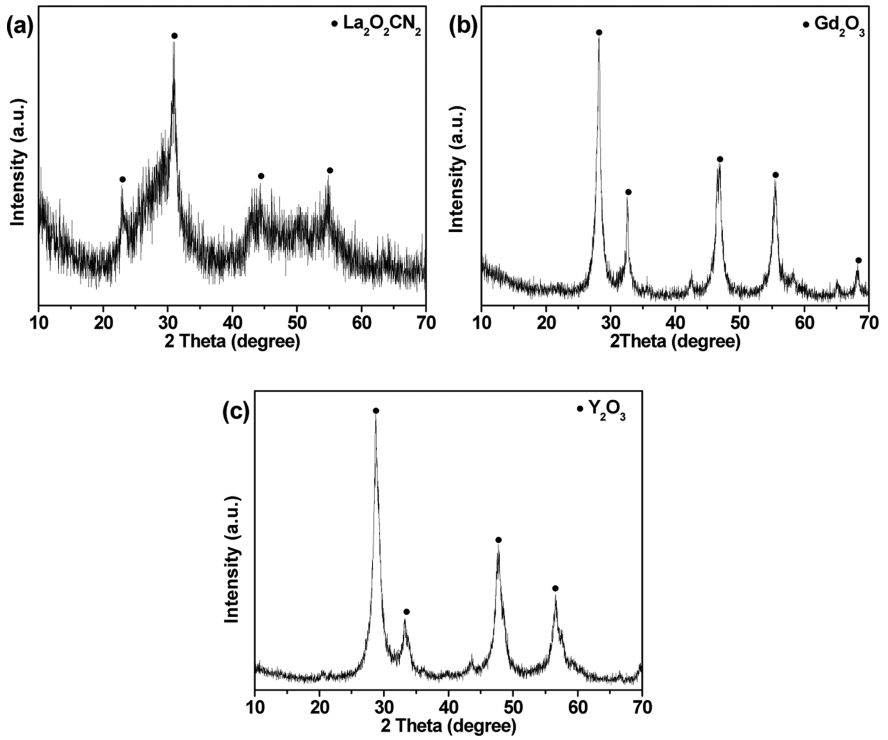

Figure 9. XRD patterns of the products obtained by calcination of the RE-CP microspheres at 550 °C for 4 h under an NH_3 atmosphere: (a) La-CP; (b) Gd-CP; (c) Y-CP.

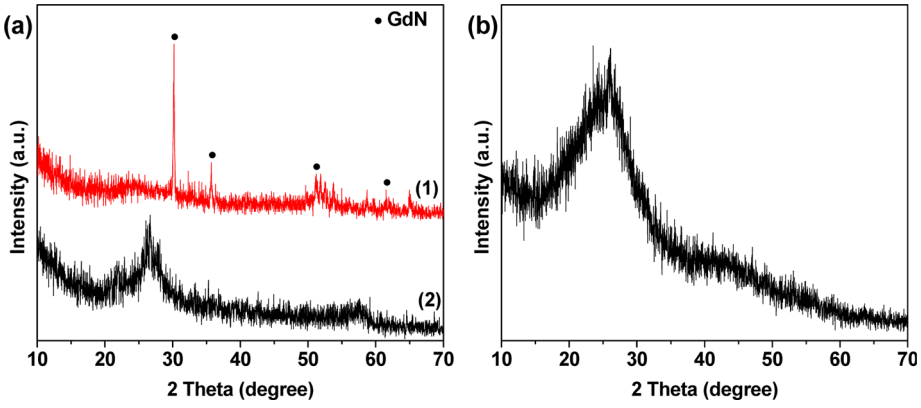

Figure 10. XRD patterns of the Gd (a1) and Y (a2) samples obtained by calcination under an NH_3 atmosphere after acid treatment: (a) 1 day for both samples; (b) 3 days for the Gd sample.

characteristic peaks of $La_2O_2CN_2$ at 2000 cm^{-1}, which is the stretching mode of C≡N, and at 1462 cm^{-1}, which is the vibration mode of CN (Figure S6c1). For the Y sample, the main peaks still appear from 1500 to 1600 cm^{-1} after calcination under N_2 and NH_3; the above results indicated that the nitride was not generated. The peak at 1383 cm^{-1} is the symmetric vibration of R-NO_2 (Figure S6d), and the peak at 1602 cm^{-1} is due to the vibration mode of C═C (sp^2), which is the characteristic peak of graphite.

Chemical surface analysis of the product obtained after calcining La-CP samples under N_2 and after acid treatment was performed using XPS, as shown in Figure S7 (Supporting Information; the inset gives the spectrum of La 3d). From the C 1s XPS spectrum of samples after acid treatment the peak at the binding energy of 286.7 eV is assigned to C−O and C−O−C, the signal at 288.5 eV is attributed to the O−C═O oxygen-containing carbonaceous band, and the deconvoluted peak centered at a binding energy of 284.6 eV is assigned to the C−C, C═C, and C−H bonds (sp^2). The XPS N 1s spectra can be deconvoluted into two peaks centered at 400 and 398.4 eV; the peak around 400 eV is assigned to the pyrrolic-N species, whereas that at 398.4 eV is attributed to the presence of pyridinic-N species.[22]

As an example of the applications of the RE-based coordination polymers, 15 mol % Yb^{3+} and 5 mol % Er^{3+} codoped Gd-CPs were prepared, and then the Gd-CPs with Yb^{3+} and Er^{3+} were calcined under atmospheres of air, N_2, and NH_3. We tested the upconversion abilities of all products upon excitation with a 980 nm laser. As can be seen in the spectrum (Figure 11), the products showed a red single peak emission band centered at λ 675 nm, corresponding to an energy-transfer process from the excited state $^4F_{9/2}$ to the ground state $^4I_{15/2}$. As many −COOH and $-NH_2$ groups are on the surface of the CP spheres, they have good biocompatibility and potential

dx.doi.org/10.1021/ic5005769 | Inorg. Chem. 2014, 53, 8278−8286

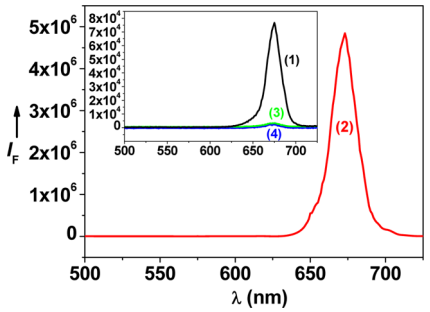

Figure 11. Upconversion luminescence spectrum of Gd-CP with Yb^{3+} and Er^{3+} and the products of Gd-CP with Yb^{3+} and Er^{3+} calcined under different atmospheres upon excitation with a 980 nm laser: (1) Gd-CP with Yb^{3+} and Er^{3+}; (2) calcination in air; (3) calcination under an N_2 atmosphere; (4) calcination under an NH_3 atmosphere.

bioapplications.[23] From the spectrum we can see that the signal of the sample calcined in air was the strongest, the precursor was secondary, and the signals of the samples calcined under N_2 and NH_3 atmospheres were very weak. Although the signal of Gd-CPs with Yb^{3+} and Er^{3+} was stronger than those for the samples calcined in air and under N_2 (Figure 11(3)), it was much weaker in comparison with that of the sample calcined in the air (Figure 11(4)). The obviously stronger upconversion efficiency of the product calcined in air in comparison to that of Gd-CP was due to crystalline materials having stronger crystal field strength in comparison to materials having low crystallinity and amorphous materials. Previous research showed that the the stronger the crystal field strength, the higher the upconversion efficiency.[24] After calcination under N_2 and NH_3, the obtained products contained carbon and GdN, and these components led to an amount of lattice distortion and surface defects on the surface of materials. These increased the instability of ions on the surfaces of the nanoparticles, reduced the symmetry of the cells, and resulted in disorder of the local area environment. These results degraded the crystal field on the surface of the material. Moreover, the surface defects acted as a path of nonradiative transition of the RE ions, which made the lifetime of RE ions shorter.[25] For the above reasons, the samples obtained in N_2 and NH_3 have low upconversion luminescence efficiency. We also tested the upconversion abilities of the products which were obtained from the Gd-CP with Yb^{3+} and Er^{3+} calcined at 750 °C under an N_2 atmosphere. As can be seen in the spectrum (Figure S8, Supporting Information), the peak emission band was seriously splitt, which can be ascribed to the fact that the calcined product has two different kinds of crystal phases. On the basis of all the results above, a higher calcination temperature did not perfect the products or their properties.

Up to now, carbon electrodes have played important roles in supercapacitors on account of their good electric conductivity, long cycle stability, and stable physicochemical properties. The carbon materials store energy through charge accumulation at the electrode/electrolyte interfaces, which allows very fast energy uptake and delivery and therefore a better power performance. The porous carbon submicrospheres have good conductivity and keep the porous structure of the original polymers, providing a short movement path for both electrolyte ions and electrons during the electrochemical process. Therefore, the obtained carbon materials may have great potential in energy storage. The porous carbon microspheres (obtained after acid treatment of the product produced after calcination of the La-CP under an N_2 atmosphere) were further applied as electrode materials for supercapacitors (Figure 12). The electrochemical properties of multihole carbon micro-

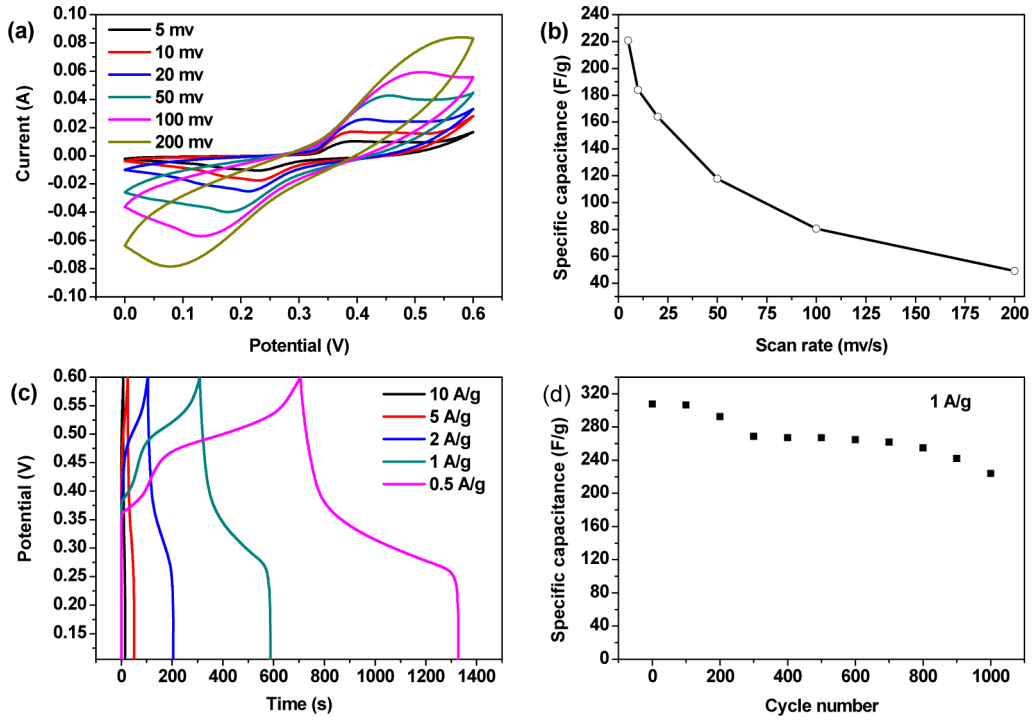

Figure 12. (a) Representative cyclic voltammetric (CV) curves of a multihole carbon microsphere electrode. (b) Calculated specific capacitances from the CV curves at different scan rates. (c) Charge/discharge curves of the multihole carbon microsphere electrode at different constant current densities. (d) Cycle life of the multihole carbon microsphere electrode at a charge/discharge current density of 1 A g^{-1} for 1000 cycles.

dx.doi.org/10.1021/ic5005769 | Inorg. Chem. 2014, 53, 8278−8286

spheres were investigated by using cyclic voltammogram (CV) and galvanostatic charge/discharge measurements within the potential window of 0−0.6 V in 6 M KOH aqueous solution with a three-electrode system. The CV curves measured at potential sweep rates of 5−200 mV s^{-1} are shown in Figure 12a. The specific capacitances of multihole carbon microspheres obtained from the CV curves are calculated by the equation $C = (\int I\, dv)/(\upsilon mV)$, where C is the specific capacitance (F g^{-1}), I is the current (A), V is the potential window (V), υ is the scan rate (mV s^{-1}), and m is the mass of the sample used for the electrochemical test (g).[26] The calculated specific capacitances at different scan rates are given in Figure 12b. The multihole carbon microspheres show specific capacitances of 220.8 and 117.7 F g^{-1} at scan rates of 5 and 100 mV s^{-1}, respectively. The charge/discharge behavior of the porous carbon microsphere electrode was also tested at current densities from 0.5 to 10 A g^{-1}. The observation of nearly symmetric potential−time curves at all current densities implies low polarization of the unique electrode.[27] The specific capacitances of multihole carbon microspheres can be calculated from the discharge curves by the equation $C = (I\,\Delta t)/(m\,\Delta V)$,[28] where I is the constant discharge current (A), Δt is the discharging time (s), and ΔV is the discharge voltage. The specific capacitances of porous carbon microspheres from the discharge curve are calculated to be 307.7 and 516.7 F g^{-1} at current densities of 1 and 0.5 A g^{-1}, respectively. The specific capacitance of porous carbon obtained at a current density of 1 A g^{-1} is comparable to those of N-doped hollow graphitic carbon spheres (260 F g^{-1}, 2 M H_2SO_4 electrolyte)[29] and N-doped carbon fibers (202.0 F g^{-1}, 6 M KOH electrolyte)[30] and is higher than that of many other carbon-based materials such as Co_3O_4/r-GO composites (163.8 F g^{-1}, 6 M KOH electrolyte).[31] The electrochemical performance of porous carbon can be explained by its porous structure and the existence of nitro groups. The porous structure expedites the transport of ions and electrons between the electrodes due to it possessing high surface area and high porosity.[32] In addition, carbon materials containing some nitrogen groups can provide pseudocapacitance and enhance the surface wettability by the electrolyte, as well as ensure a complete utilization of the exposed surface for charge storage.[33] In addition, pyridinic nitrogen, pyrrolic nitrogen, and quinone oxygen were confirmed to have the most pronounced influence on the capacitance due to their pseudocapacitive contributions.[34]

CONCLUSIONS

In conclusion, RE-based CP microspheres have been prepared by a facile microwave method, and they were calcined under different atmospheres. RE_2O_3, REN/RE_2O_3/C, REN/C, RE_2O_2CN, and carbon submicrospheres can be obtained after calcination and posttreatment. Results show that light rare earth element based CPs easily form REN on calcination under N_2 and NH_3. This method may be extended to the preparation of various composite materials with excellent properties via a facile process. There is still much room for development.

ASSOCIATED CONTENT

Supporting Information

Figures giving detailed characterization data for the products obtained in the form of XRD spectra, FTIR spectra, XPS spectra, TG-DTG curves, and an upconversion luminescence spectrum. This material is available free of charge via the Internet at http://pubs.acs.org.

AUTHOR INFORMATION

Corresponding Authors

*S.Z.: tel, +86 791 88120386; fax, +86 791 88120386; e-mail, slzhong@jxnu.edu.cn.

*L.W.: e-mail, wangleifly2006@126.com.

Notes

The authors declare no competing financial interest.

ACKNOWLEDGMENTS

S.Z. acknowledges the support of projects from the National Natural Science Foundation of China (Nos. 21201089, 21261010, 61201104), Jiangxi Provincial Department of Science and Technology (No. 2010BJB01100), and Jiangxi Provincial Education Department (Nos. GJJ11382, KJLD13021).

REFERENCES

(1) (a) Della Rocca, J.; Liu, D. M.; Lin, W. B. *Acc. Chem. Res.* **2011**, *44*, 957−968. (b) Carne, A.; Carbonell, C.; Imaz, I.; Maspoch, D. *Chem. Soc. Rev.* **2011**, *40*, 291−305. (c) Spokoyny, A. M.; Kim, D.; Sumrein, A.; Mirkin, C. A. *Chem. Soc. Rev.* **2009**, *38*, 1218−1227.

(2) Oh, M.; Mirkin, C. A. *Nature* **2005**, *438*, 651−654.

(3) Pang, M.; Cairns, A. J.; Liu, Y.; Belmabkhout, Y.; Zeng, H. C.; Eddaoudi, M. *J. Am. Chem. Soc.* **2012**, *134*, 13176−13179.

(4) Junggeburth, S. C.; Diehl, L.; Werner, S.; Duppel, V.; Sigle, W.; Lotsch, B. V. *J. Am. Chem. Soc.* **2013**, *135*, 6157−6164.

(5) Zhong, S. L.; Xu, R.; Zhang, L. F.; Qu, W. G.; Gao, G. Q.; Wu, X. L.; Xu, A. W. *J. Mater. Chem.* **2011**, *21*, 16574−16580.

(6) (a) Leonelli, C.; Mason, T. *Chem. Eng. Process.* **2010**, *49*, 885−900. (b) Dallinger, D.; Kappe, C. O. *Chem. Rev.* **2007**, *107*, 2563−2591. (c) Polshettiwar, V.; Varma, R. S. *Chem. Soc. Rev.* **2008**, *37*, 1456−1557. (d) Baghbanzadeh, M.; Carbone, L.; Cozzoli, P. D.; Kappe, C. O. *Angew. Chem., Int. Ed.* **2011**, *50*, 2−50. (e) Muthuswamy, E.; Iskandar, A. S.; Amador, M. M.; Kauzlarich, S. M. *Chem. Mater.* **2013**, *25*, 1416−1422.

(7) Jeon, Y. M.; Armatas, G. S.; Heo, J.; Kanatzidis, M. G.; Mirkin, C. A. *Adv. Mater.* **2008**, *20*, 2105−2110.

(8) Ni, Z.; Masel, R. I. *J. Am. Chem. Soc.* **2006**, *128*, 12394−12395.

(9) Umemura, A.; Diriing, S.; Furukawa, S.; Uehara, H.; Tsuruoka, T.; Kitagawa, S. *J. Am. Chem. Soc.* **2011**, *133*, 15506−15513.

(10) Zhao, D.; Wang, L.; Li, Y.; Zhang, L.; Lv, Y.; Zhong, S. *Inorg. Chem. Commun.* **2012**, *20*, 97−100.

(11) Masoomi, M. Y.; Morsali, A. *Coord. Chem. Rev.* **2012**, *256*, 2921−2943.

(12) Chaikittisilp, W.; Ariga, K.; Yamauchi, Y. *J. Mater. Chem. A* **2013**, *1*, 14−19.

(13) Hu, M.; Reboul, J.; Furukawa, S.; Torad, N. L.; Ji, Q.; Srinivasu, P.; Ariga, K.; Kitagawa, S.; Yamauchi, Y. *J. Am. Chem. Soc.* **2012**, *134*, 2864−2867.

(14) Jiang, H. L.; Liu, B.; Lan, Y. Q.; Kuratani, K.; Akita, T.; Shioyama, H.; Zong, F.; Xu, Q. *J. Am. Chem. Soc.* **2011**, *133*, 11854−11857.

(15) Yuan, D. S.; Chen, J. X.; Tan, S. X.; Xia, N. N.; Liu, Y. L. *Electrochem. Commun.* **2009**, *11*, 1191−1194.

(16) (a) Jürgens, B.; Irran, E.; Senker, J.; Kroll, P.; Müller, H.; Schnick, W. *J. Am. Chem. Soc.* **2003**, *125*, 10288−10300. (b) Hulicova, D.; Yamashita, J.; Soneda, Y.; Hatori, H.; Kodama, M. *Chem. Mater.* **2005**, *17*, 1241−1247.

(17) Wei, C.; Dai, L. M.; Roy, A.; Tolle, T. B. *J. Am. Chem. Soc.* **2006**, *128*, 1412−1413.

(18) Shen, J. F.; Yan, B.; Shi, M.; Ma, H. W.; Li, N.; Ye, M. X. *J. Mater. Chem.* **2011**, *21*, 3415−3421.

(19) Zhou, K. F.; Zhu, Y. H.; Yang, X. L.; Jiang, X.; Li, C. Z. *New J. Chem.* **2011**, *35*, 353−359.

(20) Hashimoto, Y.; Takahashi, M.; Kikkawa, S.; Kanamaru, F. *J. Solid State Chem.* **1995**, *114*, 592−594.

(21) Lei, M.; Zhao, H. Z.; Yang, H.; Li, P. G.; Tang, H. L.; Song, B.; Tang, W. H. *Diamond Relat. Mater.* **2007**, *16*, 1974−1981.
(22) Casanovas, J.; Ricart, J. M.; Rubio, J.; Illas, F.; Jiménez-Mateos, J. M. *J. Am. Chem. Soc.* **1996**, *118*, 8071−8076.
(23) (a) Zhong, S.; Ji, Y.; Xie, Q.; Wang, L.; Li, Y.; Jeong, J. H. *Mater. Lett.* **2013**, *102*−*103*, 19−21. (b) Zhou, J.; Liu, Z.; Li, F. *Chem. Soc. Rev.* **2012**, *40*, 1323−1349.
(24) Yi, G.; Lu, H. C.; Zhao, S. Y.; Ge, Y.; Yang, W. J.; Chen, D. P.; Guo, L. H. *Nano Lett.* **2004**, *4*, 2191−2196.
(25) Peng, H. S.; Song, H. W.; Chen, B. J.; Lu, S. Z.; Huang, S. H. *Chem. Phys. Lett.* **2003**, *370*, 485−489.
(26) Wu, X. L.; Wen, T.; Guo, H. L.; Yang, S. B.; Wang, X. K.; Xu, A. W. *ACS Nano* **2013**, *7*, 3589−3597.
(27) Yuan, C. Z.; Li, J. Y.; Hou, L. R.; Zhang, X. G.; Shen, L. F.; Lou, X. W. *Adv. Funct. Mater.* **2012**, *22*, 4592−4597.
(28) Lei, Z. B.; Shi, F. F.; Lu, L. *ACS Appl. Mater. Interfaces* **2012**, *4*, 1058−1064.
(29) Ma, F. W.; Zhao, H.; Sun, L. P.; Li, Q.; Huo, L. H.; Xia, T.; Gao, S.; Pang, G. S.; Shi, Z.; Feng, S. H. *J. Mater. Chem.* **2012**, *22*, 13464−13468.
(30) Chen, L. F.; Zhang, X. D.; Liang, H. W.; Kong, M.; Guan, Q. F.; Chen, P.; Wu, Z. Y.; Yu, S. H. *ACS Nano* **2012**, *6*, 7092−7102.
(31) Zhou, W.; Liu, J.; Chen, T.; Tan, K. S.; Jia, X.; Luo, Z.; Cong, C.; Yang, H.; Li, C. M.; Yu, T. *Phys. Chem. Chem. Phys.* **2011**, *13*, 14.
(32) Chen, Z.; Wen, J.; Yan, C. Z.; Rice, L.; Sohn, H.; Shen, M. Q.; Cai, M.; Dunn, B.; Lu, Y. F. *Adv. Energy Mater.* **2011**, *1*, 551−556.
(33) Li, W. R.; Chen, D. H.; Li, Z.; Shi, Y. F.; Wan, Y.; Huang, J. J.; Yang, J. J.; Zhao, D. Y.; Jiang, Z. Y. *Electrochem. Commun.* **2007**, *9*, 569−573.
(34) Hulicova-Jurcakova, D.; Seredych, M.; Lu, G. Q.; Bandosz, T. J. *Adv. Funct. Mater.* **2009**, *19*, 438−447.